

# Phase Time Crystals and Pairing in Binary Active Chiral Systems

C. Reichhardt and C. J. O. Reichhardt

*Theoretical Division and Center for Nonlinear Studies,  
Los Alamos National Laboratory, Los Alamos, New Mexico 87545, USA*

(Dated: June 30, 2026)

We introduce a class of dynamic systems we call phase time crystals consisting of a binary assembly of particles with intermediate or long-range repulsive interactions that are subjected to a circular drive of uniform chirality in which each particle species is out of phase from the other by  $180^\circ$ . As a function of the particle density and orbit radius, this system can organize into a rich variety of dynamical crystalline states, including one in which the out of phase particles form bound pairs that assemble into a triangular lattice. We also find stripe phases, overlapping packed crystals, disordered or phase glass states with no diffusion, mixed fluids, and different types of phase-separated states. We show that these states are robust against the addition of thermal fluctuations, and that the paired crystal can melt into a paired fluid. If the drive on each particle species is of opposite chirality, the system forms stripes and packed lattices, but no paired crystal is present. We demonstrate that by modifying the nature of the chiral driving, it is possible to realize numerous kinds of active molecular lattices, including dynamic square spin ice geometries and higher-order complex structures.

## I. INTRODUCTION

In equilibrium, two-dimensional systems of particles with intermediate or long-range repulsive interactions of Bessel function, Yukawa, or Coulomb type will form a triangular lattice. This process has been studied for charged colloids [1–3], magnetically interacting colloids [4], vortices in type-II superconductors [5], magnetic skyrmions [6], Wigner crystals [7], and dusty plasmas [8]. An open question is what would happen to such structures if a time-dependent component were added to the interaction. The system may still form a triangular lattice or fluid, but it is also possible that dynamic patterns could emerge in which the time dependence creates effective particle-particle interactions that are both attractive and repulsive.

One of the simplest examples of additional time-dependent interactions is the introduction of circular or chiral particle motion. Recently there has been growing interest in chiral active matter systems where the particles undergo circular motion or are themselves spinning [9–24]. Systems of active spinning particles can form large-scale rotating solids [20] with edge currents [13, 16], and can also exhibit odd viscosity and odd elasticity effects when the chirality produces transverse forces [14, 16, 22, 25–27]. Mixtures of particles that have opposite active chirality can phase separate or form mixed fluids, with edge currents appearing along the boundaries between the two species [11, 15, 18, 28–30]. In other active chiral systems, the particles undergo circular motion [15, 18, 31, 32]. Assemblies of chiral robots can organize into rotating patterns or other patterns [33, 34], and it has even been shown how to use active rotation to achieve self-assembly [35]. Most studies of chiral systems have been performed with disks or particles that have short-range or contact repulsion, so that a crystal can form only in the dense limit, but there has been some work on active particles with Lennard-Jones type interactions [36] or attractive interactions [37]. Less is known about

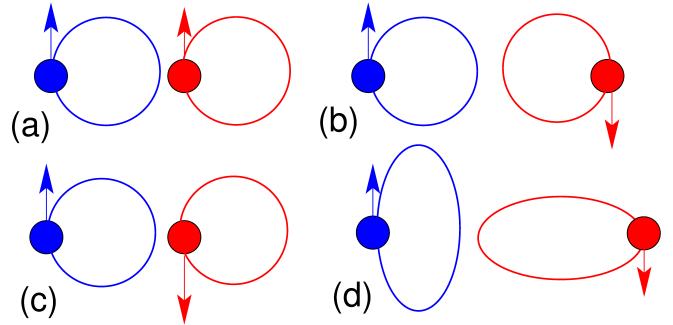


FIG. 1. Schematics illustrating active chiral driving for a binary system of particles with intermediate or long-range repulsion. (a) Two particles that both rotate in the same direction while in phase. (b) The two particles rotate in the same direction but are out of phase by  $180^\circ$ . (c) Particles that rotate with opposite chirality. (d) The particles rotate with the same chirality, are out of phase by  $180^\circ$ , and have different drive amplitudes in the  $x$  and  $y$  directions.

how chiral and non-chiral active systems would behave if the particles have intermediate or long-range repulsion; however, there are growing efforts to create active matter systems with this type of interactions [28, 38–40], including recent proposals for magnetic skyrmion systems with activity [41]. In general, if the repulsive interactions are sufficiently strong, it could be expected that the system could simply form a triangular solid by overcoming any active forces. If the activity is stronger, however, the system could remain fluid, rotate as a solid, or produce new types of ordered structures as a result of the competition between repulsion and chirality.

In this work we propose that phase time crystal states can appear in an active chiral system consisting of a binary assembly of particles with intermediate or long-range repulsion. When the chiral driving is out of phase for the two particle species, it can induce an effective attraction between the particles. In addition to triangular

lattices, this system forms paired crystals, stripe lattices, packed overlapping crystals, and glassy states, along with phase-separated and mixed fluids. We demonstrate these states for particles with Bessel function, Yukawa, and Coulomb repulsive interactions. In each case the particles form a simple triangular lattice in equilibrium, but we add a chiral driving force such that an individual particle travels in a circle with radius  $R_a$  at frequency  $\omega$ . For a fixed driving amplitude, the orbit radius increases as  $\omega$  decreases. When the particles are all driven with the same chirality and phase, as shown in Fig. 1(a), the system forms a triangular solid that rotates rigidly so that in a rotating reference frame, the particles are in a stationary triangular lattice. When we consider a binary assembly of particles rotating with the same chirality but out of phase by  $180^\circ$  with each other, as shown in Fig. 1(b), the particles organize into multiple distinct phases depending on the value of  $\omega$  and the particle density. For high  $\omega$ , when  $R_a$  is much smaller than the average lattice spacing  $a$  of the equilibrium system, the particles form a triangular lattice with non-overlapping orbits. As the drive frequency decreases, square lattices or disordered states can form instead. At lower frequencies when the active radius  $R_a$  is close to the equilibrium lattice spacing  $a$ , the system forms bound pairs of particles in which two particles that are out of phase rotate around their mutual center of mass, and the bound pairs themselves form a lattice. For other frequencies, the system can form phase-separated states with or without edge currents. When the active radius is larger than the equilibrium lattice spacing, the system can in some cases form overlapping tightly packed crystals as well as stripe crystal structures, and in other cases passes through a transient fluctuating state before settling into a dynamically disordered frozen state with no long-time diffusion. These states are robust against the inclusion of thermal fluctuations. For the paired crystal lattice, as the temperature increases the system first melts into a paired fluid where the particles remain bound into pairs of opposite phase, but the pairs can gradually diffuse. At higher temperatures, the pairs break apart and a phase-separated state emerges, while at the highest temperatures we find a mixed fluid state. At zero temperature, when the system is initialized in a disordered state, it can organize into a frozen mixture of pairs and stripes. For a binary system with opposite chirality, shown in Fig. 1(c), we find stripe lattices, overlapping crystals, and glass states, but the paired crystal state is absent. In the case of elliptical driving, illustrated in Fig. 1(d), the system can still form cross-like paired crystals as well as more complex lattices, including states similar to those found for square spin ice [42, 43] and superlattice orderings.

The phase time crystal system we propose can be viewed as an extension of the time crystal concept. Time crystals were originally proposed by Wilczek as systems in which the ground state is periodic in both space and time [44, 45], but it was soon shown that it is not possible for time crystals to form in equilibrium [46]. When

nonequilibrium effects are added, however, various types of time crystals can occur, including versions that are purely classical [47–49] or produced by non-reciprocal interactions [50]. More recently, time crystals have been proposed to occur for active matter systems with chiral interactions [51]. It has also been suggested that particles with Yukawa interactions on a dynamic substrate [52] and magnetic colloids on patterned substrates [53] could act as time-crystal-like systems. The system we describe in the present work could be realized for charged or magnetic colloidal assemblies where there is an additional chiral activity term, or using mixtures of charged particles where half of the particles also have magnetic interactions. It could also be realized using binary magnetic particle mixtures, such as skyrmion-skyrmionium mixtures, that have intermediate-range repulsion but respond differently to an oscillating field, or in charged or magnetic systems with local driving. Our results suggest new methods for self assembly and for creating an effective attraction between particles whose equilibrium interactions are purely pairwise repulsive.

## II. SIMULATION

We model a two-dimensional system of size  $L \times L$  with  $L = 36$  to  $L = 64$  that has periodic boundary conditions in the  $x$ - and  $y$ -directions. The system contains  $N$  particles at a density of  $\rho = N/L^2$ , and is evenly divided between two particle species, with  $N/2$  particles of species A and  $N/2$  particles of species B. The particles have repulsive interactions, independent of species type, and are initially placed in a triangular lattice. We first consider particles with intermediate length repulsion represented by a modified Bessel function,  $V(R_{ij}) = F_0 K_0(R_{ij})$ , where  $F_0$  is a constant and  $\mathbf{R}_{i(j)}$  is the position of particle  $i(j)$ . The Bessel function decays exponentially at large distances and describes interactions between vortices in type-II superconductors, skyrmions in chiral magnets, and is also a good approximation for a variety of screened-charge systems [54]. We consider two other types of interaction potentials and find that they give similar results. The first is a repulsive Yukawa potential,  $V(R_{ij}) = C e^{-R_{ij}}/R_{ij}$ , where  $C$  is a constant prefactor. The second is a long-range Coulomb potential,  $V(R_{ij}) = Q/R_{ij}$ , and in this case we employ the Lekner summation technique for computational efficiency [55, 56], as used previously for driven charge motion on random substrates [57]. If thermal fluctuations are sufficiently small, particles with any of these interaction potentials will form a triangular lattice. We introduce active chiral driving terms  $\mathbf{F}^A$  and  $\mathbf{F}^B$  that cause individual particles of species A or B, respectively, to move in a circle of radius  $R_a$  at a frequency  $\omega$ .

The overdamped equation of motion for particle  $i$  is

$$\eta \frac{d\mathbf{R}_i}{dt} = - \sum_{j \neq i}^N \nabla V(R_{ij}) + \mathbf{F}_i^A \delta(\sigma_i - 1) + \mathbf{F}_i^B \delta(\sigma_i) \quad (1)$$

where the damping coefficient is set to  $\eta = 1.0$  and particles of species A are assigned  $\sigma_i = 1$  while particles of species B are assigned  $\sigma_i = 0$ . In the initial triangular lattice, the particles are placed such that every other lattice site is occupied by a species A or a species B particle to give maximal mixing, where the A and B particle species can be subjected to different chiral driving protocols as shown in Fig. 1. For the main part of this work, we consider the protocol in Fig. 1(b) where the particles have the same chirality and same driving amplitude but are out of phase by  $180^\circ$ . In this case, species A is subjected to the rotating drive  $\mathbf{F}^A(t) = A \sin(\omega t) \hat{y} + A \cos(\omega t) \hat{x}$ , while species B has a rotating drive of  $\mathbf{F}^B(t) = -A \sin(\omega t) \hat{y} - A \cos(\omega t) \hat{x}$ . In Fig. 1(a) where  $\mathbf{F}^A = \mathbf{F}^B$ , the system effectively contains only one particle species and all of the particles rotate as a coherent solid. When the particles are driven with opposite chirality, as in Fig. 1(c), species A has the same drive as above but the species B drive is changed to  $\mathbf{F}^B(t) = A \cos(\omega t) \hat{y} + A \sin(\omega t) \hat{x}$ . Unless otherwise stated, the ac drive amplitude is set to  $A = 1.0$ . We also consider the case shown in Fig. 1(d) where the  $x$  and  $y$  driving amplitudes have different values to create elliptical orbits.

Throughout this work, we use a simulation time step of size  $\delta t = 0.005$ , and we report time in units of the period  $\tau = 2\pi/\omega$  of the ac drive. We measure the fraction of sixfold-coordinated particles without regard to species identity,  $P_6 = (1/N) \sum_{i=1}^N \delta(z_i - 6)$ , where  $z_i$  is the coordination number of particle  $i$  obtained from a Voronoi tessellation. For a triangular lattice,  $P_6 = 1.0$ . We also measure the mean square displacement versus time per particle,  $d(t) = (1/N) \sum_{i=1}^N |R_i(t) - R_i(t_0)|^2$ , where  $R_i(t)$  is the position of particle  $i$  at time  $t$  and the measurement is made from a reference time  $t = t_0$ . In a fluid,  $d(t)$  grows linearly with time, while for a crystal or frozen state,  $d(t)$  saturates to a constant value.

### III. CHIRAL SYSTEM OUT OF PHASE

We first consider the situation from Fig. 1(b) where particles with Bessel function interactions have the same direction of chirality, but the two species are out of phase by  $180^\circ$ . We begin with the high frequency limit where the orbit radius is much smaller than the average particle spacing. In Fig. 2(a,b) we illustrate the particle configurations and trajectories for a system with  $\rho = 0.208$  at  $\omega = 0.012$ . For this density, the non-driven system forms a triangular lattice with a spacing of  $a = 2.19$ , while the particle orbits at  $\omega = 0.012$  have an average radius of  $R_a = 0.4$ , so there is no overlap of adjacent orbits. Before taking the images in Fig. 2(a,b), we wait  $1 \times 10^4$  simulation time steps, which is sufficient time for any initial transients to subside and for the system to settle into a steady cyclic state. We illustrate the trajectories during 20 to 50 ac drive cycles. Here the steady state consists of a distorted triangular lattice of monomers of rotating par-

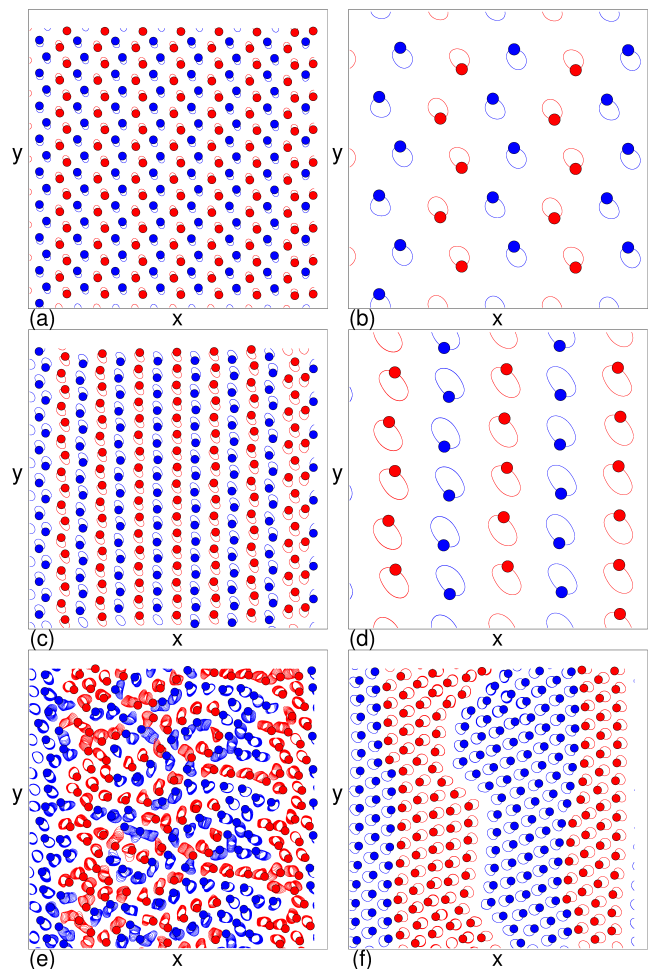


FIG. 2. Particle positions (circles) and trajectories (lines) for Bessel function particles at density  $\rho = 0.208$  where species A is blue and species B is red. The particles are subjected to circular driving of the same chirality but are out of phase by  $180^\circ$  as shown in Fig. 1(b); the drive amplitude is  $A = 1.0$ . Except where stated, the trajectories are obtained during an interval of 20 to 50 ac drive cycles after the system has been allowed to evolve for  $10^4$  simulation time steps. (a) A distorted triangular lattice (phase I) at  $\omega = 0.012$ . (b) A blow-up of panel (a) showing more clearly that the orbits are slightly elliptical. (c) At  $\omega = 0.008$  the system forms a stripe lattice (phase II) with more elliptical orbits. (d) A blow-up of panel (c). (e) At early times for  $\omega = 0.0075$ , the system breaks up into a transient fluid. (f) The same as panel (e) after  $5 \times 10^4$  ac driving cycles have elapsed and the system has settled into a phase-separated solid (phase III).

ticles (phase I). In Fig. 2(b) we show a zoomed in view of a smaller subsection of the system that more clearly indicates that the two species are out of phase with each other in their orbits, which are not completely circular but are somewhat elliptical. The slight noncircularity of the orbits is a result of the particle-particle interactions: since the particles are out of phase with each other, they can move slightly further apart from each other and minimize their interaction energy by distorting the orbit shapes.

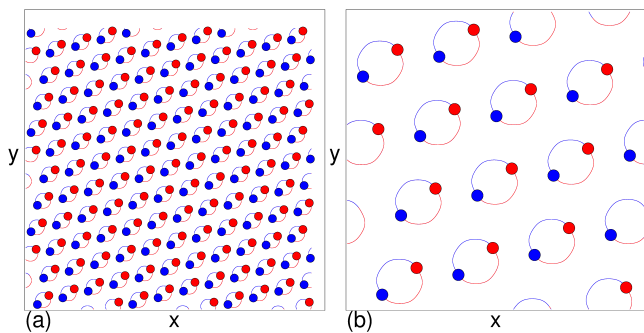


FIG. 3. (a) Particle positions (circles) and trajectories (lines) where species A is blue and species B is red for the out of phase Bessel function particles at  $\rho = 0.208$  from Fig. 2 in the paired crystal state (phase IV) at  $\omega = 0.0055$ , where the particles share orbits as pairs and these pairs then form a higher-order crystal. (b) A blow-up of panel (a).

At higher values of  $\omega$  (not shown), we obtain the same structure as in Fig. 2(a,b), but the orbits become smaller and more circular, and the triangular lattice formed by the particles becomes less distorted. The particles repeat the exact same trajectory during each drive cycle, so there is no diffusion. The type of ordering we observe can have some dependence on the initial particle placement, as discussed in a later section. When we lower the driving frequency, the orbit size increases and the system settles into different monomer patterns, as shown in Fig. 2(c,d) at  $\omega = 0.008$ , where the orbits are more noticeably elliptical and the overall ordering can be described as a stripe lattice (phase II). All of the ellipses for the orbits of both particle species are tilted in the same direction. At even lower frequencies, the elliptical orbits become increasingly elongated and the system breaks up into a transient disordered fluid phase, illustrated in Fig. 2(e) for  $\omega = 0.0075$ . Over time the particles organize into a phase separated solid (phase III), shown in Fig. 2(f) for the  $\omega = 0.0075$  system after several thousand ac driving cycles have elapsed. In the phase separated state, each particle species forms a triangular lattice, the orbits become much more circular, and there is no long-time diffusion.

Over the range  $0.0045 < \omega < 0.007$  at the same density of  $\rho = 0.208$  as in Fig. 2, we find an interesting paired crystal state (phase IV). Figure 3(a) shows an example of the paired crystal at  $\omega = 0.0055$ . Pairs of particles that are out of phase share a single orbit, and these pairs then form a larger scale triangular lattice. The zoomed in view of a portion of the sample in Fig. 3(b) illustrates more clearly that the paired particles are in the same orbit but are out of phase with each other, and are traveling around a center of mass point. The range of  $\omega$  over which the paired crystal can form depends on  $\rho$  and  $A$ . At early times, the system can form a square lattice of pairs that then undergo a series of transient rearrangements before settling into a steady state triangular lattice. The paired crystal state can emerge when the orbit

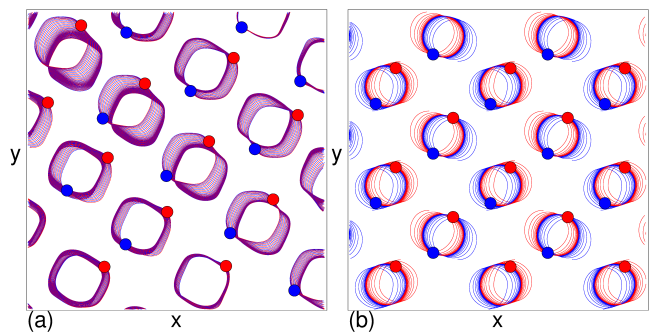


FIG. 4. Particle positions (circles) and trajectories (lines) where species A is blue and species B is red for the out of phase Bessel function particles at  $\rho = 0.208$  from Fig. 2 in the paired crystal state (phase IV). (a) At early times for  $\omega = 0.005$  the orbit shape has a square character. After some rearrangements occur, the system settles into a triangular lattice with nearly circular orbits. (b) Early time evolution at  $\omega = 0.005$  for weaker particle-particle interactions of  $F_0 = 0.2$ , showing that there is an effective attraction between particles that brings the particles together into paired orbits.

radius  $R_a$  becomes large enough that two adjacent orbits would overlap; however, by sharing the same orbit, the two particle species can form a lattice containing orbits that are smaller than the lattice constant of the paired state. Since the lattice constant goes as  $a \propto \rho^{-1/2}$ , and the paired particle density is half that of the unpaired particle, the lattice of the paired state is larger by  $\sqrt{2}$  than that of the unpaired state. For larger  $\omega$  in the paired state, the orbits exhibit small distortions away from being circular.

In Fig. 4(a) we show that at early times in the paired crystal state at  $\omega = 0.005$ , the orbits have a more square shape. After a transient period, the system rearranges and settles into a triangular paired lattice. Figure 4(b) shows the early time evolution for a system still at  $\omega = 0.005$  but with a reduced particle-particle interaction strength of  $F_0 = 0.2$ . The out of phase particles are initially in separate orbits but are effectively attracted to each other in pairs, forming the paired crystal at later time.

For  $0.00325 \leq \omega \leq 0.0045$ , the particle orbits become so large that the paired crystal is not able to form and instead a phase-separated state emerges; however, since the orbits are large, the system has a fluid-like behavior with edge currents flowing along the boundaries between the two phases. In Fig. 5(a) we show the early time configurations and trajectories at  $\omega = 0.004$ , where there is some pairing of particles but there is fluid-like motion throughout the system. At later times in the steady state, Fig. 5(b) shows that a phase-separated state has emerged, but the particle orbits are larger than the average spacing between particles and there is considerable motion throughout the system. This phase-separated fluid (phase V) contains some local triangular ordering, and the particles can gradually move to the phase sep-

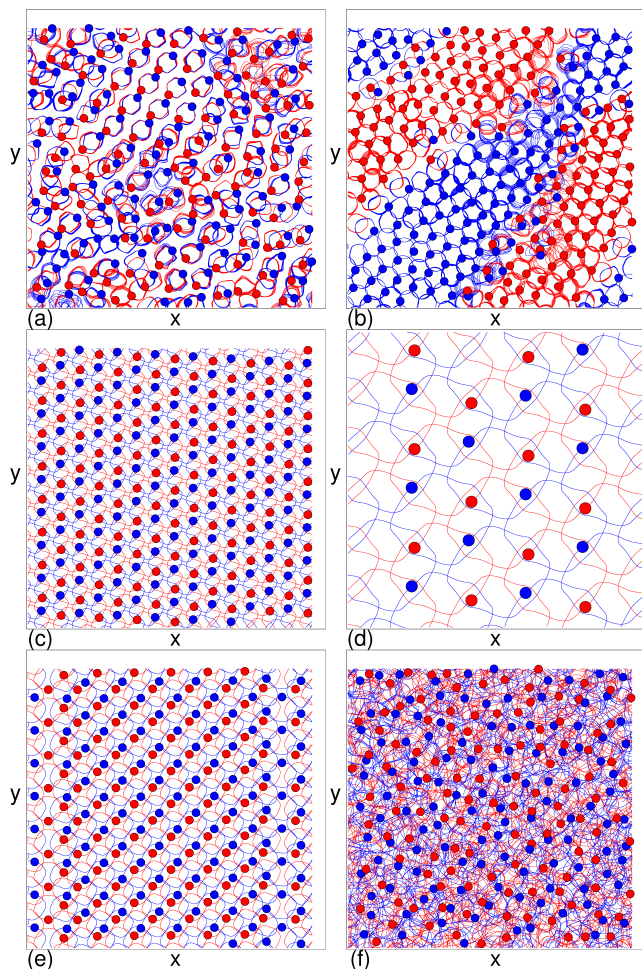


FIG. 5. Particle positions (circles) and trajectories (lines) where species A is blue and species B is red for the out of phase Bessel function particles at  $\rho = 0.208$  from Fig. 2. (a) The early time configuration and trajectories at  $\omega = 0.004$  showing fluid motion. (b) The steady state configuration for  $\omega = 0.004$  where the system forms a phase-separated fluid (phase V). (c) An overlapping packed crystal (phase VI) at  $\omega = 0.0025$ . (d) A blow-up of panel (c). (e) The overlapping packed crystal at  $\omega = 0.00325$ , where the shape of the orbit is different compared to panels (c, d). (f) The mixed fluid state (phase VII) for  $\omega = 0.002$ .

aration boundaries where a slight amount of mixing of particle species occurs. For  $0.00235 \leq \omega \leq 0.00325$ , we find an ordered overlapping packed crystal state (phase VI), as shown in Fig. 5(c) for  $\omega = 0.0025$ . The close-up view of this state in Fig. 5(d) indicates that even though the particle orbits are larger than the average particle spacing, the system can still form a dynamically ordered state. The overlapping crystal state at a slightly higher frequency of  $\omega = 0.003$  in Fig. 5(e) has orbits of altered shape compared to the  $\omega = 0.0025$  system in Fig. 5(c,d). For  $\omega < 0.00235$ , the system forms a mixed fluid (phase VII), illustrated at  $\omega = 0.002$  in Fig. 5(f). This mixed fluid state does not phase separate even at long times.

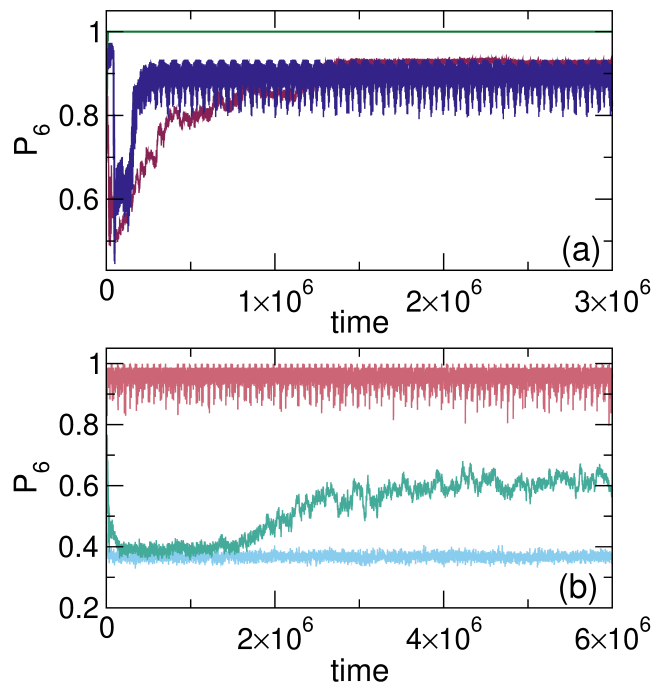


FIG. 6.  $P_6$  versus time for the out of phase Bessel function particles at  $\rho = 0.208$  from Fig. 2. (a) Green: distorted triangular lattice (phase I) at  $\omega = 0.012$ . Purple:  $\omega = 0.0075$  where the system forms a fluid that gradually phase separates into a phase separated solid (phase III). Dark blue: paired crystal (phase IV) at  $\omega = 0.0055$ . (b) Teal: phase separated fluid (phase V) at  $\omega = 0.004$ . Pink: overlapping packed crystal (phase VI) at  $\omega = 0.0025$ . Light blue: mixed fluid (phase VII) at  $\omega = 0.002$ .

For much lower driving frequencies, the system can form laned states, which will be studied in a different work.

To get a better idea of the dynamics, in Fig. 6(a) we plot  $P_6$  versus time for the system from Figs. 2 to 5 at three values of  $\omega$ . For  $\omega = 0.012$ ,  $P_6 \approx 1.0$  and the system immediately forms a distorted triangular lattice (I) as shown in Fig. 2(a,b). At  $\omega = 0.0075$ , initially the particles disorder and have  $P_6 \approx 0.5$  in the transient fluid state shown in Fig. 2(e), but  $P_6$  increases over time and saturates to  $P_6 \approx 0.9$  in the phase-separated state shown in Fig. 2(f). The system does not completely order in the phase-separated state due to the presence of topological defects on the boundary separating the two phases. In general, this state can be described as a phase-separated solid (III). For  $\omega = 0.0055$ , after an initial period of transient motion the system settles into a paired crystal state (IV) with  $P_6 = 0.88$ . The Voronoi construction is based on the instantaneous locations of the individual particles, and in the paired crystal state,  $P_6$  is slightly depressed during a portion of each cycle, causing the average value of  $P_6$  to be noticeably lower than 1.0 even though a Voronoi construction performed on the center of mass of each pair would show  $P_6 \approx 1.0$ .

In Fig. 6(b), we plot  $P_6$  versus time for the disordered

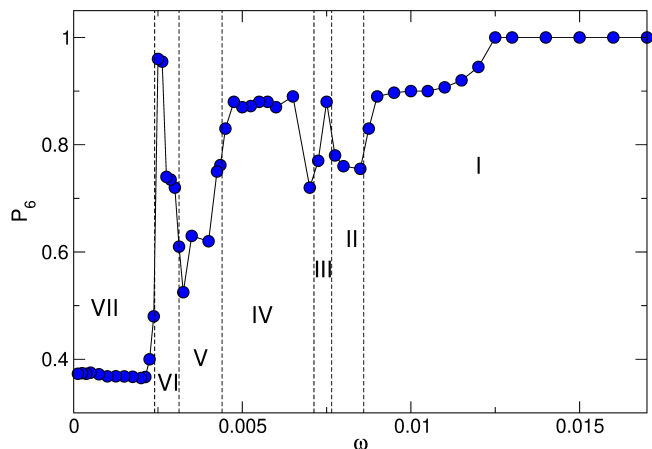


FIG. 7. The steady state value of  $P_6$  vs  $\omega$  for the out of phase Bessel function particles at  $\rho = 0.208$  from Fig. 2. Vertical lines separate the different phases we identify, which are numbered from high to low frequency. I: distorted triangular crystal. II: stripe lattice. III: phase-separated solid. IV: paired crystal. V: phase-separated fluid. VI: overlapping packed crystal. VII: mixed fluid.

or phase separated fluid state (V) at  $\omega = 0.004$ . At early times the system starts off in a mixed fluid state with  $P_6 \approx 0.4$ , as shown in Fig. 5(a), but then becomes better phase separated, as illustrated in Fig. 5(b), causing  $P_6$  to increase to  $P_6 \approx 0.6$ . This phase-separated state is not as well ordered as the phase-separated solid that appears for  $\omega = 0.0075$ , and it is better described as a phase-separated fluid. For  $\omega = 0.0025$  in the overlapping packed crystal state (VI) shown in Fig. 5(c,d),  $P_6$  is high again. The fluctuations in  $P_6$  are produced when the particles approach each other more closely during portions of the ac cycle, disrupting the order locally. In the mixed fluid (VII) from Fig. 5(f) at  $\omega = 0.002$ ,  $P_6$  is close to  $P_6 = 0.39$  and does not change with time.

Although the Voronoi construction only takes into account the instantaneous positions of the particles, and not their velocities, it still captures the changes that occur between states and can distinguish between ordered and disordered states. In Fig. 7 we plot  $P_6$  versus  $\omega$  for the system from Fig. 6, where we take the average value of  $P_6$  only after the system has reached a steady state. The phases we distinguish are distorted triangular crystal (I), stripe lattice (II), phase-separated solid (III), paired crystal (IV), phase-separated fluid (V), overlapping packed crystal (VI), and the mixed fluid state (VII). For  $\omega > 0.0086$ , we find a disordered triangular lattice (I) that gradually becomes less distorted as  $\omega$  increases. Over the range  $0.0086 < \omega < 0.012$ , the Voronoi algorithm gives an average value of  $P_6 = 0.9$  because the distortions of the triangular lattice are sufficiently large that a finite number of non-sixfold coordinated polygons are present in the system. For  $\omega > 0.012$ , the triangular lattice is less distorted, all of the Voronoi polygons are hexagons, and  $P_6 = 1.0$ . When  $0.0075 < \omega < 0.0086$ , we

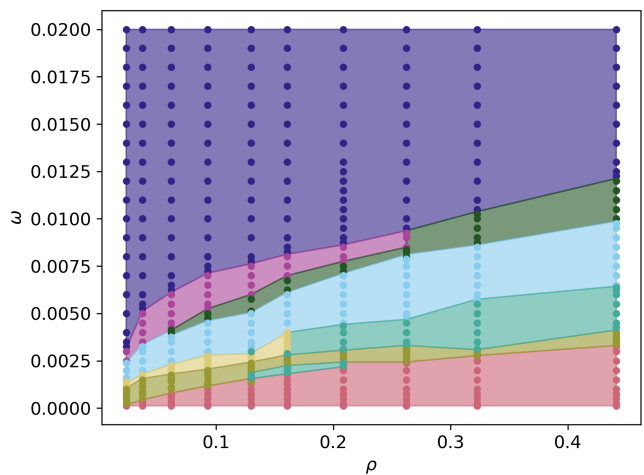


FIG. 8. Phase diagram for the out of phase Bessel function particles from Fig. 2 as a function of  $\omega$  vs  $\rho$ . Dark blue: distorted triangular crystal (I). Light purple: stripe lattice (II). Dark green: phase-separated solid (III). Light blue: paired crystal (IV). Light green: phase-separated fluid (V). Dark yellow: overlapping packed crystal (VI). Light yellow: overlapping stripe or glassy states (VI). Red: mixed fluid (VII). Example animations of motion in phases I, II, III, IV, VI, and VII as well as in the noninteracting limit at  $\rho = 0.0926$  appear in the supplemental material [58].

observe a stripe lattice state (II) of the type illustrated in Fig. 2(c,d), and  $P_6$  takes a lower value. In the phase-separated solid (III) around  $\omega = 0.0075$ ,  $P_6$  increases to nearly  $P_6 \approx 0.9$  since for this frequency the system phase separates into only two domains, while at a lower frequency of  $\omega = 0.00725$ , multiple phase separated domains are present, which increases the amount of phase boundary in the system and consequently depresses the value of  $P_6$ . For  $0.0045 < \omega < 0.0072$  in the paired crystal state (IV),  $P_6$  is close to  $P_6 \approx 0.87$  but has a dip near  $\omega = 0.007$  due to the presence of a small number of particles that do not form pairs. In the phase-separated fluid (V),  $P_6$  is close to  $P_6 \approx 0.6$ , which is considerably higher than the random mixed fluid (VII) value of  $P_6 \approx 0.38$ . Between the phase-separated fluid and the random mixed fluid we find a packed overlapping crystal (VI) with a maximum value of  $P_6 \approx 0.95$ , but at higher values of  $\omega$  in phase VI  $P_6$  drops to  $P_6 = 0.75$ , due to distortions of the Voronoi tessellation that occur when particles get relatively close together. There is also a small region from  $0.002 < \omega < 0.0025$  in which the system is better described as a partially phase-separated fluid, which is not highlighted in Fig. 7. For lower  $\omega$ , the system remains in the mixed fluid state (VII) with  $P_6 \approx 0.38$ .

From the images of the particle motion and the behavior of  $P_6$ , we use a range of particle densities to construct the phase diagram shown in Fig. 8 as a function of  $\omega$  versus  $\rho$ . We highlight the distorted triangular crystal (I), stripe lattice (II), phase-separated solid (III), paired crystal (IV), phase-separated fluid (V), overlapping packed

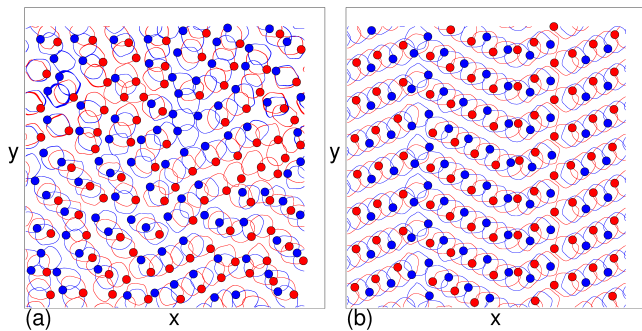


FIG. 9. Particle positions (circles) and trajectories (lines) where species A is blue and species B is red for the out of phase Bessel function particles at  $\rho = 0.161$  from the phase diagram in Fig. 8. (a) A dynamical frozen stripe glass state (VI) at  $\omega = 0.0035$ . (b) The system is more ordered at  $\omega = 0.00325$ .

crystal (VI), and the mixed fluid (VII). For  $\rho < 0.2$ , we observe overlapping stripe or glassy-like phases that we lump into phase VI, and for lower  $\omega$ , there are additional types of overlapping packed crystals. As  $\rho$  increases, the lower boundary of the distorted triangular crystal (I) shifts to higher  $\omega$ . This is due to the decrease in the equilibrium lattice constant which goes as  $a \propto \rho^{-1/2}$ , so as  $\rho$  becomes larger, it is necessary to apply a higher  $\omega$  to prevent the active orbits from overlapping. For  $\rho > 0.3$ , the monomer stripe lattice state (II) disappears due to the high elastic energy cost of elliptical orbits, which increases with increasing  $\rho$ . The paired crystal and overlapping crystal are present over the entire range of densities shown in Fig. 8, and generally the phase boundaries shift to higher values of  $\omega$  with increasing  $\rho$ . For lower  $\rho$ , the extent of the liquid phase is reduced and a greater number of dynamically frozen states appear. In principle, in the absence of thermal fluctuations for sufficiently small  $\rho$ , the particles are so far apart that they are only weakly interacting, so the system should always settle into a frozen orbit state.

In Fig. 9(a) we show an example of a dynamical frozen stripe glass state at  $\omega = 0.0035$  and  $\rho = 0.161$ . In this case the paired particles overlap in chains, with the particle species alternating along the length of the chain. In general, glassy states such as this one undergo a period of transient rearrangements before settling into a state where there is no long-time diffusion. At these lower densities and frequencies, the difference separating an ordered overlapping crystal from a glassy state is a dynamical commensuration effect that determines which orbits keep the moving particles as far apart from each other for as much of the time as possible. For example, at  $\rho = 0.208$ , when  $\omega = 0.0055$  the individual particles are close enough together that the ratio of the orbit radius to the equilibrium lattice spacing is  $R_a/a \approx 1$ , while at a frequency  $\omega = 0.00275$  that is half as large,  $R_a/a \approx 2$ . In each case, when  $R_a/a$  is close to an integer, an overlapping crystal appears. The implication is that higher order overlapping lattices could emerge whenever  $R_a/a = n/m$

for integer  $n$  and  $m$ , and indeed, at the lower densities we observe a variety of overlapping crystal states. When the commensurate conditions are not met, the system forms either a fluid or a glassy state. The interaction energy is higher in the glassy state than in the fluid, and since the interaction energy increases as  $\rho$  increases, the fluid state is favored at higher densities and we do not observe frozen glass states for  $\rho > 0.2$ . Frozen glasses do appear at lower  $\rho$  when the particle-particle spacing is larger. In some cases, the stripe glasses exhibit a noticeable remnant of ordering, as shown in Fig. 9(b) at a lower frequency of  $\omega = 0.00325$ . The ordering in the stripe glass or other overlapping packed crystal states could also be affected by the periodic boundary conditions of our system. Geometric confinement could produce other types of crystal states, and the system could be fluid-like along the edges of the confinement but crystalline in the bulk. There is a transient time that must elapse before a glassy system reaches a frozen state, and the length of this transient is expected to increase with increasing system size, so it is possible that in a sufficiently large system the glassy arrangement would never reach a truly frozen state on observable time scales. We find, however, that the transient motion in the glassy state occurs in bursts and that the system spends some time frozen before undergoing intermittent rearrangements, a dynamical process that will be explored elsewhere.

In Fig. 10(a) we show the particle configurations and trajectories in the paired crystal (IV) state for the system from Fig. 8 at  $\rho = 0.0926$  and  $\omega = 0.004$ . Figure 10(b) shows that for the same density at  $\omega = 0.0025$ , the system organizes into a stripe glass, while in Fig. 10(c) at  $\omega = 0.00175$ , there is an overlapping packed crystal (VI). In Fig. 10(d) at  $\omega = 0.0015$ , the system freezes into a disordered glass state. When  $\omega = 0.00125$ , as in Fig. 10(e), another overlapping packed crystal (VI) appears that is different from the one found at  $\omega = 0.00175$ . There are also other ordered stripes and even dimer states that can form, such as the state shown in Fig. 10(f) at  $\rho = 0.0617$  and  $\omega = 0.00225$  which can be described as a dimer lattice. At smaller densities, the periodic boundary conditions can start to affect the ordering; however, when we consider the same sets of parameters in larger systems with  $L = 48$  and  $L = 72$ , we generally obtain the same sets of phases. In some cases the stripe glass states can be more ordered or disordered when the system is made larger, but the other ordered phases remain robust.

#### IV. SCREENED COULOMB INTERACTIONS

We next consider the case of particles with screened Coulomb or Yukawa interactions. We observe a similar set of phases as for the Bessel function interactions; however, the coefficient in the interaction potential must take different values in the two systems to give the same phases. For  $V(r) = C \exp(-r)/r$ , if we take  $\rho = 0.208$  and  $\omega = 0.00525$ , where we found a paired crystal (IV)

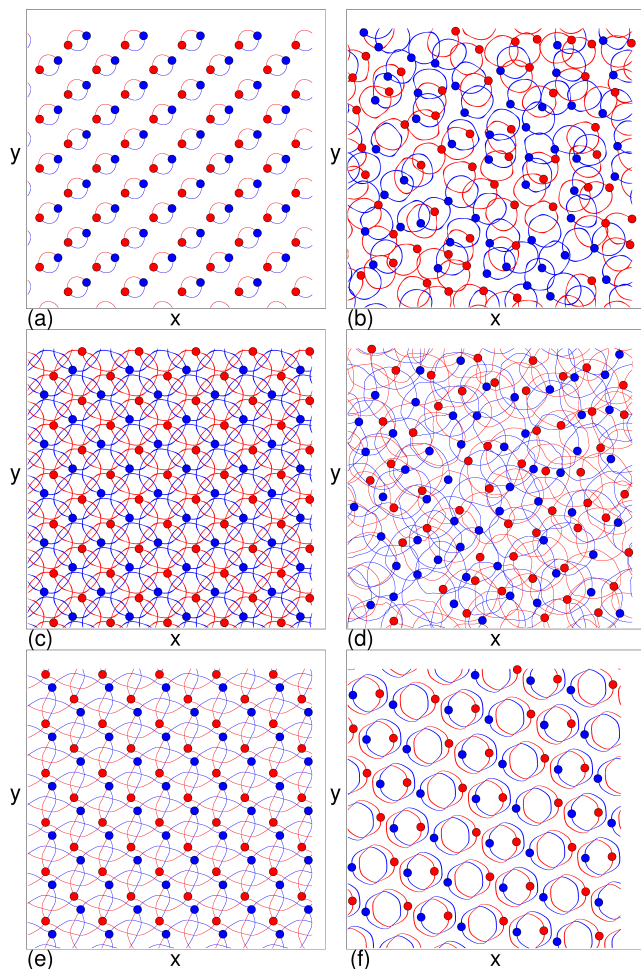


FIG. 10. Particle positions (circles) and trajectories (lines) where species A is blue and species B is red for the out of phase Bessel function particles from Fig. 8. (a) Paired crystal (IV) at  $\rho = 0.0926$  and  $\omega = 0.004$ . (b) Stripe glass at  $\rho = 0.0926$  and  $\omega = 0.0025$ . (c) Overlapping packed crystal (VI) at  $\rho = 0.0926$  and  $\omega = 0.00175$ . (d) Disordered glass at  $\rho = 0.0926$  and  $\omega = 0.0015$ . (e) Overlapping packed crystal (VI) at  $\rho = 0.0926$  and  $\omega = 0.00125$ . (f) Dimer lattice at  $\rho = 0.0617$  and  $\omega = 0.00225$ .

for the Bessel function interaction, we instead find a disordered phase-separated state (III) at  $C = 0.5$ , as shown in Fig. 11(a). In this state, the particles are able to form closed circular orbits, but diffusion can still occur. For  $C = 0.2$ , we find a paired crystal (IV) as shown in Fig. 11(b). If  $C$  is too small, the system forms a disordered frozen state, as shown at  $\omega = 0.035$  and  $C = 0.02$  in Fig. 11(c). For the same low  $C = 0.02$  at  $\omega = 0.025$  in Fig. 11(d), there is an overlapping packed crystal (VI). In general, for smaller  $C$ , the fluid phase is reduced in extent and a greater variety of overlapping packed crystal states can form. If we consider larger values of  $C$ , many of the same phases are still present but have shifted to different densities. These results indicate that the phases we observe should be robust over a wide range of intermediate

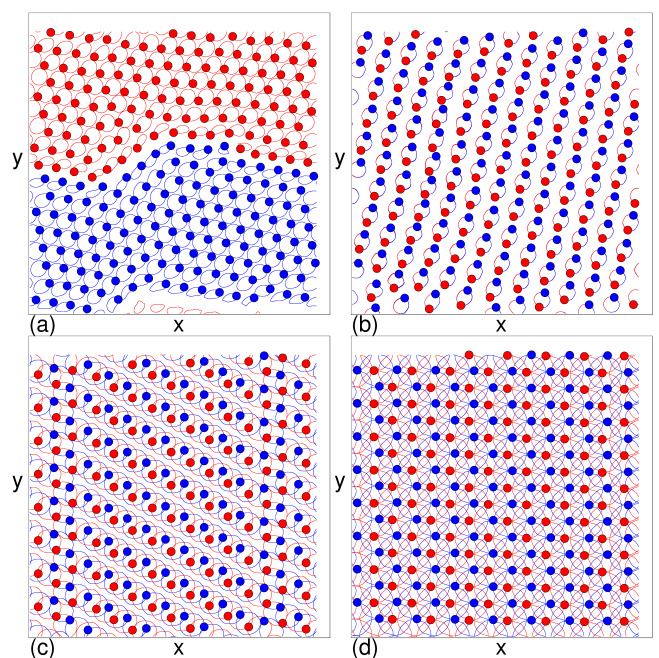


FIG. 11. Particle positions (circles) and trajectories (lines) where species A is blue and species B is red for the out of phase Yukawa particles with interactions of the form  $V(r) = C \exp(-r)/r$  at  $\rho = 0.208$ . (a) A phase-separated solid (III) at  $C = 0.5$  and  $\omega = 0.00525$ . (b) A paired crystal (IV) at  $C = 0.2$  and  $\omega = 0.00525$ . (c) A frozen disordered state at  $C = 0.02$  and  $\omega = 0.035$ . (d) An overlapping packed crystal (VI) at  $C = 0.02$  and  $\omega = 0.025$ .

repulsive particle-particle interaction potentials.

## V. COUNTER-ROTATING MIXTURES

We return to the Bessel function interactions and next consider a counter-rotating system in which one particle species rotates in one direction and the other species rotates in the opposite direction, as shown in Fig. 1(c). Although some of the dynamical phases we find are similar to those from the system where the two particle species are rotating in the same direction but out of phase, there are numerous differences. We use the Bessel function interaction to make a clear comparison with the out of phase system from Fig. 2. In Fig. 12(a) we show the particle locations and trajectories for a counter-rotating system at  $\rho = 0.208$  and  $\omega = 0.011$ , where we highlight only a subset of the system for clarity. We find a distorted triangular lattice (I) where the particles have non-overlapping elliptical orbits and the ellipses of each species are tilted in a different direction. For these parameters, the out of phase system forms a similar state. At high frequencies, the orbits of adjacent particles are not large enough to overlap, so the pairwise repulsion between the particles dominates, producing a similar triangular lattice regardless of whether the particles are ro-

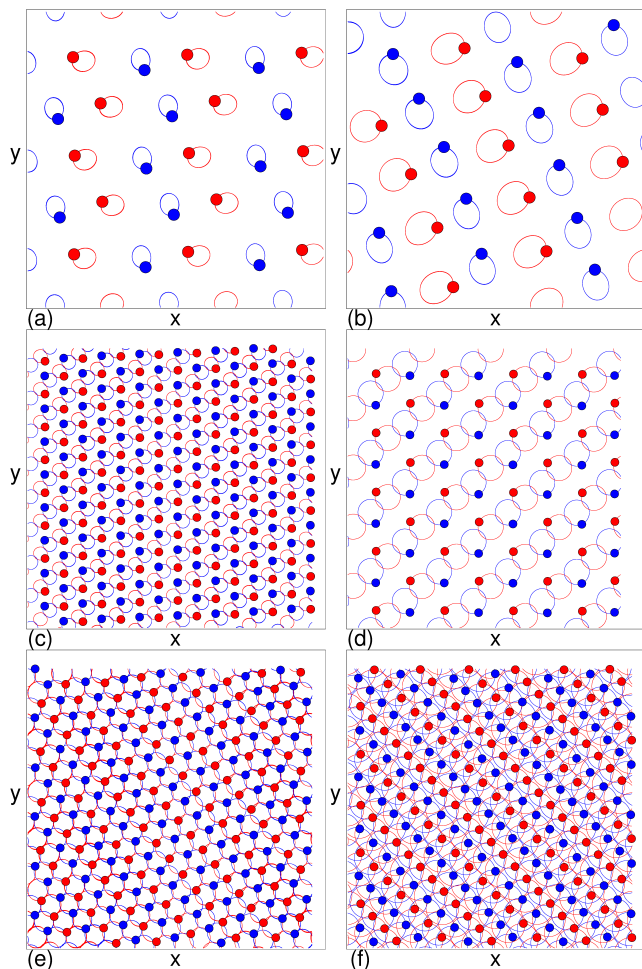


FIG. 12. Particle positions (circles) and trajectories (lines) where species A is blue and species B is red for the counter-rotating Bessel function particles shown in Fig. 1(c). (a) A blow-up view of the distorted triangular crystal (I) at  $\rho = 0.208$  and  $\omega = 0.011$ . (b) A blow-up view of the stripe lattice (II) at  $\rho = 0.208$  and  $\omega = 0.008$ . (c) An ordered chain state at  $\rho = 0.208$  and  $\omega = 0.006$ . (d) An ordered chain state at  $\rho = 0.0617$  and  $\omega = 0.0035$ . (e) An overlapping lattice with some dislocations at  $\rho = 0.208$  and  $\omega = 0.004$ . (f) An overlapping packed crystal (VI) at  $\rho = 0.208$  and  $\omega = 0.0025$ .

tating in the same direction out of phase or are counter-rotating.

In Fig. 12(b), at  $\omega = 0.008$  the counter-rotating system forms a non-overlapping stripe-like lattice with larger orbits that are still elliptical with two tilt directions. When  $\omega = 0.006$ , where a paired crystal (IV) appears for the out of phase system, Fig. 12(c) shows that the counter-rotating system forms a periodic array of chains with overlapping orbits, indicating that the different species have effective dipolar or anisotropic interactions with each other. Formation of a chain structure permits the particles of opposite chirality to move in such a way that two neighboring particles never approach each other closely throughout the cycle. The pairwise repulsion also

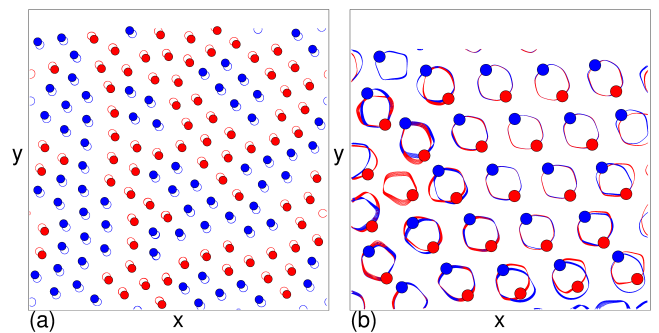


FIG. 13. Particle positions (circles) and trajectories (lines) where species A is blue and species B is red for the out of phase Bessel function particles from Fig. 1(b) where the initialization protocol has been changed and the particles are placed at random non-overlapping positions. The images are obtained in the steady state after the system has passed through a transient disordered triangular lattice. (a) At  $\rho = 0.208$  and  $\omega = 0.01$ , we find a distorted and partially phase-separated triangular lattice. (b) At  $\rho = 0.208$  and  $\omega = 0.00525$ , a zoomed in view shows that the system forms a paired crystal containing some unpaired particle defects.

produces a well-defined spacing between adjacent chains. In general, we find that for parameters at which the out of phase particles are in a paired crystal state (IV), there is an overlapping stripe state for counter-rotating particles. We show another example of such an overlapping stripe state in Fig. 12(d) at  $\omega = 0.0035$  and  $\rho = 0.0617$ . It is easy to understand why the counter-rotating particles do not form a paired crystal, since if particles with opposite chirality were to share the same orbit, they would collide and break apart the orbit. The counter-rotating particles exhibit some phases that do not appear in the out of phase system. For example, in Fig. 12(e) for  $\rho = 0.208$  and  $\omega = 0.004$ , we find an overlapping lattice that contains some dislocations. For the same system at  $\omega = 0.0025$  in Fig. 12(f), an ordered overlapping packed crystal (VI) appears. In general, there are a greater amount of ordered dynamical states for the counter-rotating particle mixtures than for the out of phase particles, since the opposite chirality allows the particles to remain further apart throughout the driving cycle compared to when the particles have the same chirality but are out of phase. It would also be possible to explore other driving protocols in which the phase difference between the particles of the same chirality is not  $180^\circ$  but has some other value, and this could produce an even richer set of phases.

## VI. INITIAL PREPARATION

Up to this point we have initialized the system in a triangular lattice where each species occupies every other lattice site in an ordered tiling. To test the effect of the initialization protocol on the results, we place the parti-

cles at randomly chosen non-overlapping positions, with the same 50:50 distribution of species A and B but with no ordering in the starting locations of each species. At high  $\omega$ , we still obtain a distorted triangular crystal (I) as in the phase diagram of Fig. 8, but the arrangement of the species in the crystal is more mixed. Species A and B are randomly distributed inside the crystal state instead of forming wavy vertical lines as in Fig. 2(a). For these high frequencies, the orbits are sufficiently small that the system behaves like a collection of point particles that are insensitive to the chirality, so the system simply crystallizes without regard to particle species. In Fig. 13(a), we show the particle configurations and trajectories for an assembly of out of phase Bessel function particles at  $\rho = 0.208$  and  $\omega = 0.01$ , where we find a distorted triangular lattice that has some amount of phase separation. The stripe crystal of Fig. 2(b) has been replaced by a disordered mixed triangular lattice state due to the change in the initialization protocol. The two states appear over nearly the same sets of parameters for both initialization protocols. For values of  $\rho$  and  $\omega$  where the paired crystal occurs in Fig. 8, the randomly initialized system still forms pairs, but there are a small number of particles that are unable to find a pair, resulting in the emergence of trapped monomers. There is also a longer transient time for the randomly initialized system before it settles in to the mostly paired state. In Fig. 13(b), we show the particle configuration and trajectories at  $\rho = 0.208$  and  $\omega = 0.00525$  for the randomly initialized system after it has settled into a steady state. Most of the particles are paired but there are a few monomer defects present. At lower frequencies and densities, changing the initialization protocol to random gives stripe glass states and overlapping crystal states that are more disordered compared to the triangular lattice initialization protocol, but in general, at the lowest densities, the system still reaches a dynamical frozen state.

## VII. PARTICLES WITH COULOMB INTERACTIONS

We return to our original initialization protocol and consider the effect of using particles with long-range Coulomb interactions, beginning with particles that have the same chirality but that are driven out of phase by  $180^\circ$ . We find that the dynamics are similar to those of the shorter-range repulsively interacting systems with Bessel or Yukawa interactions. In Fig. 14, we show the phase diagram for the Coulomb system as a function of  $\omega$  vs  $\rho$ , where we find the same phases from before: distorted triangular crystal (I), stripe lattice (II), phase-separated solid (III), paired crystal (IV), overlapping packed crystal and overlapping phase-separated fluid (V), stripe or glassy states (VI), and mixed fluid (VII). The overall shape of the phase diagram is similar to what we find for the intermediate-range repulsive Bessel function particles in Fig. 8. In general, the phase-separated states

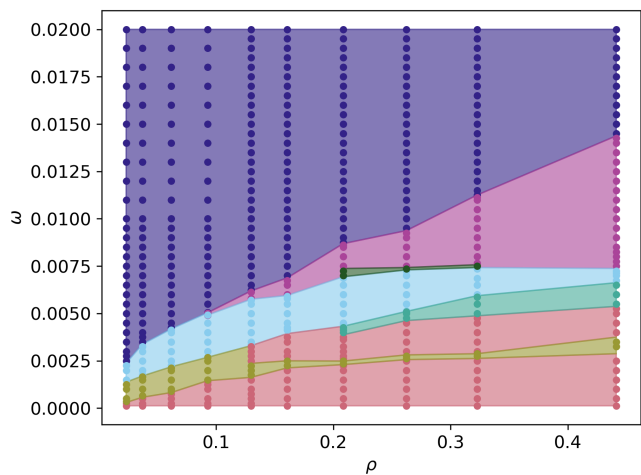


FIG. 14. Phase diagram for the out of phase Coulomb particles as a function of  $\omega$  vs  $\rho$ . Dark blue: distorted triangular crystal (I). Light purple: stripe lattice (II). Dark green: phase-separated solid (III). Light blue: paired crystal (IV). Light green: phase-separated fluid (V). Dark yellow: overlapping packed crystal and overlapping stripe or glassy states (VI). Red: mixed fluid (VII).

are less prominent for the Coulomb particles than for the Bessel particles. Note that in Fig. 14, we do not distinguish between the ordered overlapping packed crystal and the stripe glass states.

In Fig. 15(a) we show the particle positions and trajectories for the out of phase Coulomb particles from Fig. 14 at  $\rho = 0.0923$  and  $\omega = 0.004$ . Here there is a paired crystal lattice (IV) that has the same features as the paired crystals observed for Bessel and Yukawa interacting particles. At the same density and frequency of  $\rho = 0.0923$  and  $\omega = 0.004$ , if the particles instead counter-rotate as in Fig. 1(c), Fig. 15(b) shows that an ordered chain state appears. In general we do not observe paired crystal states for counter-rotating particles with opposite chirality for the Coulomb system. For the out of phase Coulomb particles from Fig. 14, Fig. 15(c) illustrates the overlapping packed crystal (VI) that appears at  $\rho = 0.0923$  at  $\omega = 0.002$ , while in Fig. 15(d), we find an overlapping stripe crystal (VI) at  $\rho = 0.0923$  and  $\omega = 0.00225$  in the same system.

Another method for categorizing the different phases is by measuring the mean square displacement  $d(t)$  versus time. In general, for crystal phases,  $d(t)$  shows a short-time transient behavior followed by saturation to a constant value, since there is no long-time diffusion. In Fig. 16, we plot  $d(t)$  for the out of phase Coulomb system from Fig. 14 at  $\rho = 0.208$ . For the paired crystal state (IV) at  $\omega = 0.005$ ,  $d(t)$  is flat at long times. We observe similar behavior in the overlapping packed crystal and frozen glass phases since none of these states has any long-time diffusion in the frozen regime. The transient time required to reach a disordered frozen glass state is generally longer than the time needed to form a

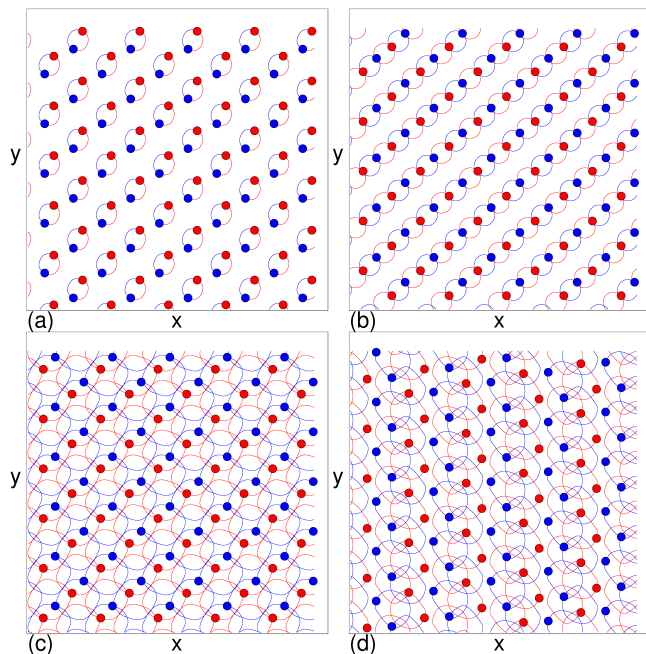


FIG. 15. Particle positions (circles) and trajectories (lines) where species A is blue and species B is red for the Coulomb particles from the system in Fig. 14. (a) Paired crystal (IV) at  $\rho = 0.0923$  and  $\omega = 0.004$  for out of phase particles. (b) A chain lattice state at the same  $\rho = 0.0923$  and  $\omega = 0.004$  as in panel (a) but for counter-rotating particles. (c) Overlapping packed crystal at  $\rho = 0.0923$  and  $\omega = 0.002$  for out of phase particles. (d) Overlapping stripe crystal at  $\rho = 0.0923$  and  $\omega = 0.00225$  for out of phase particles.

crystal state. For the mixed fluid (VII) at  $\omega = 0.002$ ,  $d(t)$  increases linearly with time, indicating that regular diffusion is occurring. The phase-separated fluid at  $\omega = 0.004$  exhibits diffusive motion at early times and a more rapid increase in  $d(t)$  at intermediate times as the system phase separates. This is followed by regular diffusion at long times in the phase-separated state. Along the boundary between the domains of different particle species in the phase-separated fluid, there is edge transport where particles can temporarily move ballistically; particles can also move in and out of the boundary. For the phase-separated solid (III, not shown), the form of  $d(t)$  is similar to that found for the paired crystal (IV), where  $d(t)$  reaches a plateau value at long times since there is no long-time diffusion.

### VIII. THERMAL FLUCTUATIONS AND MELTING IN THE PAIRED CRYSTAL STATE

We next address the question of how stable the phases we observe are against the introduction of thermal fluctuations. In general we find that the phases are robust in the presence of a finite temperature, and that interesting melting behaviors occur that will be explored in another work. Here we focus on the paired crystal state, which is

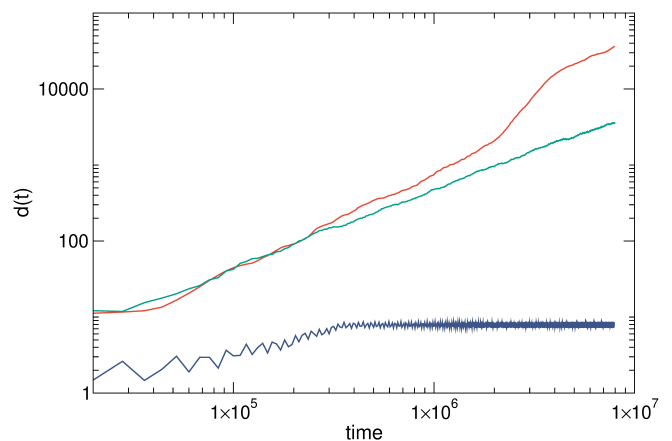


FIG. 16. The root mean square displacement  $d(t)$  vs  $t$  for the out of phase Coulomb system from Fig. 14 at  $\rho = 0.208$ . Blue: the paired crystal (IV) state at  $\omega = 0.005$ . Red: the phase-separated fluid (V) at  $\omega = 0.004$ . Green: the mixed fluid (VII) at  $\omega = 0.002$ .

not only stable and robust against thermal fluctuations, but also can persist up to temperatures that are higher than the melting temperature  $T_m$  of the nondriven lattice.

We represent the thermal forcing with Langevin kicks that have the properties  $\langle F^T(t) \rangle = 0.0$  and  $\langle F_i^T(t) F_j^T(t') \rangle = 2\eta k_B T \delta_{ij} \delta(t - t')$ , and we consider the out of phase Coulomb interacting system in the paired crystal state (IV) at  $\rho = 0.09529$  and  $\omega = 0.004$ . When the particles are passive and the ac driving is zero, the system forms a triangular lattice in which the onset of diffusion occurs at a temperature  $T_m$  which we define as the equilibrium melting temperature. When we make the system active by turning on the ac driving, the paired crystal remains robust up to temperatures that are slightly higher than  $T_m$ . In Fig. 17(a), we show the particle positions and trajectories at  $T/T_m = 0.33$ . The orbits show some thermal smearing, but the pairs are persistent and the paired crystal lattice remains intact. At  $T/T_m = 0.67$  in Fig. 17(b), the thermal smearing has widened and a single unpaired defect has appeared, but apart from this highly localized distortion the crystal structure remains present and there is no long-time diffusion. Figure 17(c) shows the motion at  $T/T_m = 1.33$ , where long-time diffusion is occurring. Most of the particles remain in bound pairs, so the system is best described as a paired fluid. This result indicates that the binding energy for the pairing of the particles is larger than the elastic energy of the paired crystal lattice. For  $T/T_m = 2.0$  in Fig. 17(d), most of the pairs have broken apart and strong diffusion occurs throughout the system. Some phase separation appears, and we find some transient pairing along the boundaries of the phase domains. At higher temperatures than what is illustrated here, the system forms a mixed fluid. A number of open questions would be interesting to explore in future work. These

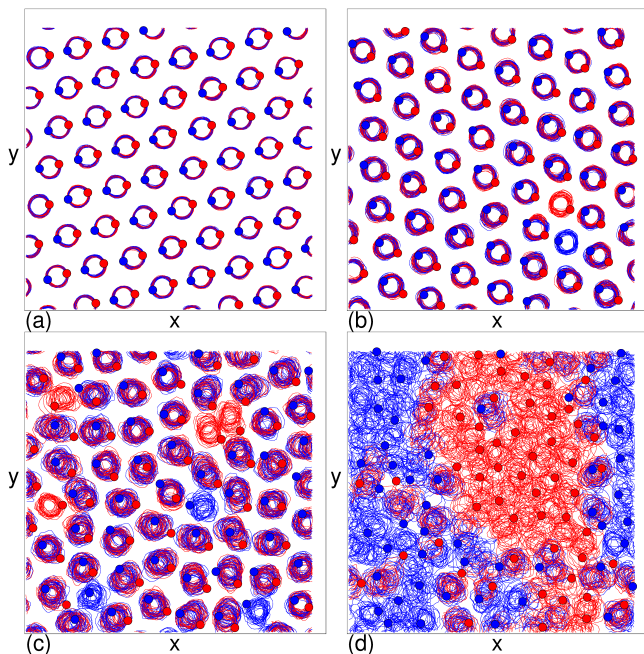


FIG. 17. Particle positions (circles) and trajectories (lines) where species A is blue and species B is red for the out of phase Coulomb particles from Fig. 14 at  $\rho = 0.0923$  and  $\omega = 0.004$ , where a paired crystal (IV) forms at zero temperatures. We examine thermal effects at different values of  $T/T_m$ , where  $T_m$  is the temperature at which the non-driven system first shows long-time diffusion. (a) At  $T/T_m = 0.33$  there is a paired crystal. (b) At  $T/T_m = 0.67$  there is also a paired crystal. (c) At  $T/T_m = 1.33$  a paired fluid appears. (d) At  $T/T_m = 2.0$  there is a phase-separated fluid.

include whether the paired crystal to paired fluid transition is associated with a paired hexatic state, such as the hexatic phases recently observed in charged colloidal systems with additional activity [40]. It would also be interesting to determine if there is multiple-step melting, as well as the transport properties of the paired fluid, how the other phases melt, and how the counter-rotating system melts.

### IX. PHASE TIME MOLECULAR CRYSTALS

We next demonstrate how to realize a rich variety of other kinds of phase time crystals as well as what we call phase time molecular crystals, and show that distinct types of paired crystals can occur. We specifically consider the case where the two species have the same chirality but are driven out of phase by  $180^\circ$  and have different elliptical driving orbits, as shown in Fig. 1(d). The chiral driving on species A is  $\mathbf{F}^A(t) = A \sin(\omega t) \hat{y} + B \cos(\omega t) \hat{x}$ , and on species B it is  $\mathbf{F}^B(t) = -B \sin(\omega t) \hat{y} - A \cos(\omega t) \hat{x}$ . For  $A = 2.0$  and  $B = 1.0$ , species A executes an elliptical orbit with its long axis aligned in the  $y$  direction, while species B rotates in an elliptical orbit aligned with the  $x$  direction. Under this out of phase elliptical driving,

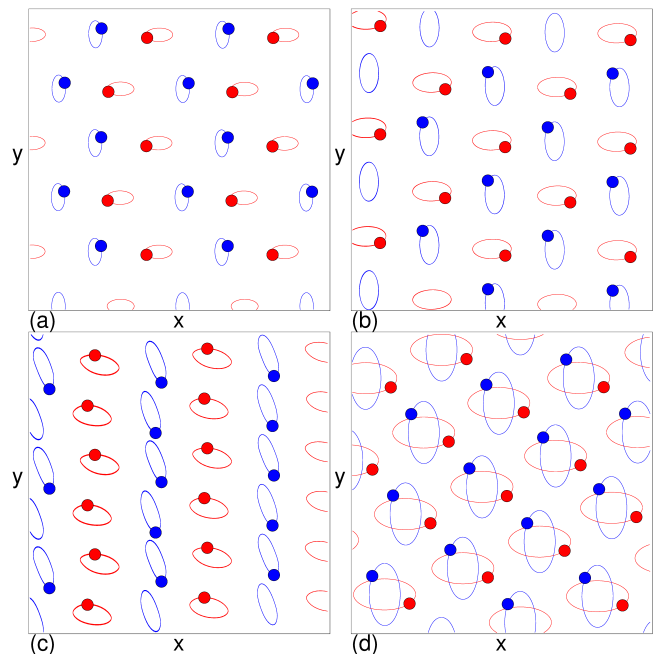


FIG. 18. Zoomed in view of particle positions (circles) and trajectories (lines) where species A is blue and species B is red for the out of phase elliptically driven Coulomb particles at  $\rho = 0.208$ . As in Fig. 1(d), the species A ellipses are aligned in the  $y$  direction and the species B ellipses are aligned in the  $x$  direction. (a) A distorted triangular crystal at  $\omega = 0.02$ . (b) A square spin ice lattice at  $\omega = 0.00145$ . (c) Elongated elliptical motion at  $\omega = 0.0125$ . (d) A paired crystal with a cross shape at  $\omega = 0.008$ .

we observe variations of the same phases found for out of phase circular driving. In Fig. 18(a) we show a subsection of the  $\omega = 0.02$  and  $\rho = 0.208$  system where the orbits are small enough that a distorted triangular lattice (I) state appears even though the individual particle orbits are clearly elliptical. At  $\omega = 0.0145$  in Fig. 18(b), we find what we call a spin ice-like lattice, while in Fig. 18(c) a variation of this lattice appears at  $\omega = 0.0125$ . The terminology “spin ice lattice” is selected in analogy to two-dimensional particle-based artificial spin ices in which particles are placed in elongated traps that have alternating alignment along the  $x$  and  $y$  directions [42, 43]. Figure 18(d) shows that at  $\omega = 0.008$ , there is a paired crystal state in which the elliptical orbits overlap to create a cross-like geometry. For out of phase circular orbits with a drive amplitude of  $A = 1.0$  at  $\omega = 0.008$  and  $\rho = 0.208$ , the phase diagram in Fig. 14 indicates that a non-overlapping stripe lattice appears. For the out of phase elliptical orbits in Fig. 18(d), the larger  $ac$  amplitude along one direction for each particle makes the orbits effectively larger, permitting pairing to persist up to higher driving frequencies compared to circular orbits.

If we consider particles with opposite chirality and elliptical drives, the paired states are no longer present. Instead we find chain crystal states of the type shown in Fig. 19(a) at  $\rho = 0.208$  and  $\omega = 0.008$ . A zoomed in view

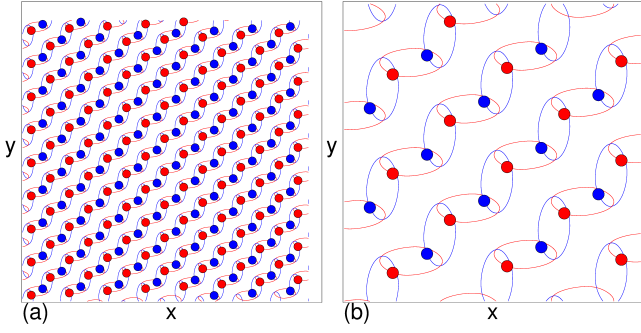


FIG. 19. (a) Particle positions (circles) and trajectories (lines) where species A is blue and species B is red for counter-rotating elliptically driven Coulomb particles at  $\rho = 0.208$  and  $\omega = 0.008$ , showing a paired crystal with a cross shape. (b) A zoom in of panel (a).

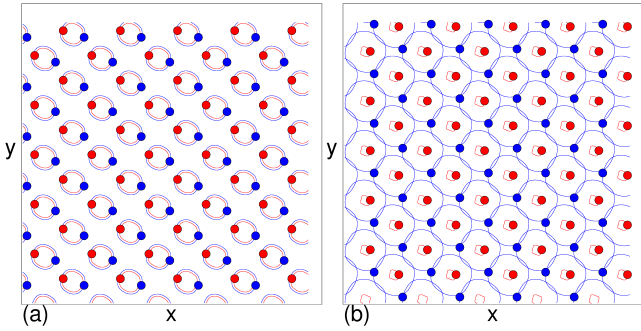


FIG. 20. Particle positions (circles) and trajectories (lines) where species A is blue and species B is red for out of phase Coulomb particles where the driving is circular but of unequal amplitude in the two species. (a)  $\rho = 0.208$  and  $\omega = 0.006$ , where species A has a drive amplitude of  $A_A = 1.2$  and species B has a drive amplitude of  $A_B = 1.0$ . (b)  $\rho = 0.098$  and  $\omega = 0.00375$ , where species A has a drive amplitude of  $A_A = 2.0$  and species B has a drive amplitude of  $A_B = 0.5$ .

of this state appears in Fig. 19(b). This state has similarities to the chain state that appears for counter-rotating particles with circular rather than elliptical driving.

To further test the robustness of the pairing, we consider a system with circular orbits of different sizes. The drive amplitude is  $A_A = 1.2$  for species A and  $A_B = 1.0$  for species B, so that the two species execute orbits of different radii. It is still possible for a paired crystal state to form even for uneven orbit sizes, as shown in Fig. 20(a) at  $\rho = 0.208$  and  $\omega = 0.006$ , where both particle species share a common orbit center point in each pair. Figure 20(b) shows the same system at  $\rho = 0.098$  and  $\omega = 0.004$  where species A has a drive amplitude of  $A_A = 2.0$  and species B has an amplitude of  $A_B = 0.5$ . In this case, the inner orbit of the species B particles has a square symmetry, which corresponds to the square symmetry of the large-scale lattice.

For out of phase particles with the same chirality under elliptical driving, we find additional phases at low

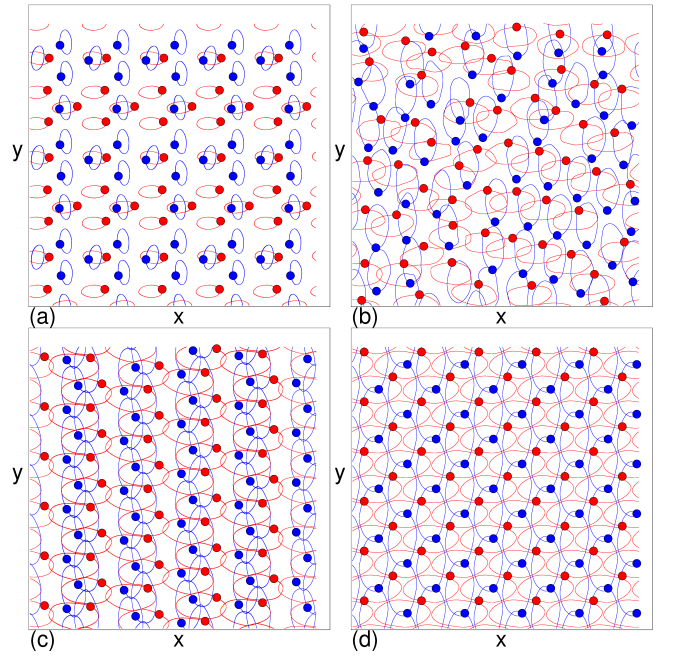


FIG. 21. Particle positions (circles) and trajectories (lines) where species A is blue and species B is red for out of phase elliptically driven Coulomb particles with  $A = 1.0$  and  $B = 2.0$  for both particle species. The species A orbits are aligned in the  $y$  direction and the species B orbits are aligned in the  $x$  direction. (a) A superlattice ordering of monomers and paired states at  $\rho = 0.098$  and  $\omega = 0.00675$ . (b) A stripe glass state at  $\rho = 0.098$  and  $\omega = 0.00375$ . (c) A stripe crystal at  $\rho = 0.098$  and  $\omega = 0.00325$ . (d) An overlapping packed crystal at  $\rho = 0.098$  and  $\omega = 0.003$ .

particle densities. In Fig. 21, where  $A = 1.0$  and  $B = 2.0$  for both species, at  $\rho = 0.098$  and high  $\omega$  we observe a distorted triangular crystal state with non-overlapping orbits similar to that shown in Fig. 18(b). When we lower the driving frequency, we observe superlattice ordering of paired and unpaired particles as illustrated in Fig. 21(a) at  $\omega = 0.00675$ . In this state, every other row of paired particles has an alternating tilt, and every paired particle is surrounded by six monomers. For  $0.004 < \omega < 0.00675$  we observe a paired cross crystal, while for  $\omega = 0.00375$  the system forms a stripe glass as shown in Fig. 21(b). At  $\omega = 0.00325$  we find the stripe crystal shown in Fig. 21(c), while for even lower  $\omega = 0.003$  the overlapping packed crystal state shown in Fig. 21(d) appears. If we further lower the frequency, we find some additional regimes of overlapping packed crystals and mixed fluids.

For certain parameter windows, there can be precession of the particle orbits. The precession is purely transient when both species are driven at the same frequency, as has been considered throughout this work. This is illustrated in Fig. 22(a) for  $\rho = 0.098$  and  $\omega = 0.007$  in the same out of phase elliptically driven Coulomb particle system from Fig. 21. Here the monomers undergo large scale rotation around the paired crosses until the sys-

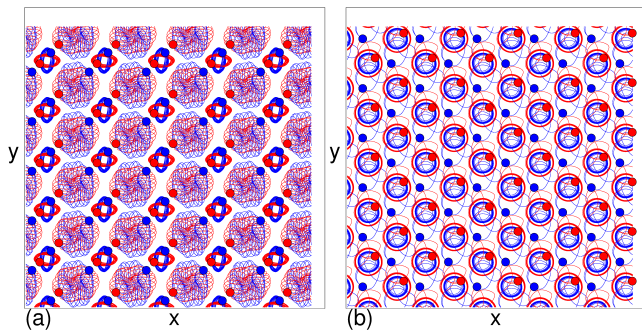


FIG. 22. Particle positions (circles) and trajectories (lines) where species A is blue and species B is red for out of phase Coulomb particles at  $\rho = 0.098$  showing transient behavior for elliptical or circular driving. (a) A system with elliptical driving where  $A = 2.0$  and  $B = 1.0$ , and where  $\omega = 0.007$  for both species, showing the transient motion of a mixture of monomers and a paired state. (b) A system with circular driving at  $A = 1.0$  but different driving frequencies of  $\omega_A = 0.00348$  for species A and  $\omega_B = 0.0035$  for species B. The system forms a transient paired crystal before jumping into a monomer state. The image shows the jumping process.

tem eventually settles into the superlattice state shown in Fig. 21(a). If the driving frequencies of the two species are not exactly matched, we can also see transient states that have additional motion. For example, if we consider out of phase circularly driven Coulomb particles, as shown in Fig. 14 there is a paired crystal state at  $\rho = 0.098$  spanning the range  $0.0027 < \omega < 0.005$ . We can drive each species at a frequency chosen from this window such that the driving frequencies are similar but not identical. In Fig. 22(b) we show the case where species A is driven at  $\omega_A = 0.00348$  while species B is driven at  $\omega_B = 0.0035$ . Although the frequencies are relatively close together, they are not close enough to stabilize the paired crystal state. At short times the system enters the paired crystal configuration, but at some point the particles jump out of this state and form a disordered monomer state. The trajectories during this transition process are illustrated in Fig. 22(b). We have considered other combinations of driving frequencies and find that when  $\omega_A/\omega_B$  is an integer or rational ratio, it is possible to stabilize a paired state, while in other cases, there can be a periodic transition between disordered and partially ordered states over time. These additional frequency effects will be explored in another work.

## X. DISCUSSION

The pairwise particle-particle interactions we consider in this work favor formation of a triangular lattice in a static system. The pattern formation we observe arises through the competition of the pairwise interaction and the activity of the driven particles. One way to understand this is that the activity creates a time-averaged

flattening of the effective pairwise interactions. For example, it is known that in systems where the interactions are purely repulsive but where there are at least two length scales present, such as through flattening of the interaction at some radius or through the presence of a step in the potential, numerous mesoscale patterned states can appear such as bubbles or stripes [59, 60]. Such shoulder or core-corona type interaction potentials have been proposed for describing stripe and bubble states of electrons in magnetic fields [61]. Bubble and stripe states can also occur when the particle interactions have competing short-range attraction and long-range repulsion terms [62–64].

Several of the states we observe may represent examples of transitions from a fluctuating state to a non-fluctuating or absorbing state, or to a periodically reversible state [65]. In a study of active circularly moving disks, Lei *et al.* [17] showed that the system starts off in a fluctuating state but over time either reaches a dynamically frozen state or remains in a fluctuating state, so that the frozen state is an example of an absorbing state. For periodically sheared disks, the transition from a fluctuating state to a cyclic reversible state as a function of shear amplitude and/or particle density is known as random organization [66]. Similar transitions from fluctuating to reversible states have also been demonstrated for strongly interacting periodically sheared amorphous solids [67, 68], indicating that absorbing phases can appear in strongly interacting systems. In our system, the glassy frozen states typically have long transient times during which the system transitions from a fluctuating state into a dynamically frozen state. These glassy frozen states would be the most similar to the dynamical frozen states for the chiral system described by Lei *et al.* [17]; however, since our system has long-range repulsion, the structures we observe are more stripe-like.

Our system can be viewed as an extension of the concept of a time crystal in that the ordered structures we find are periodic in both space and time. In equilibrium systems, pattern formation arises as a result of minimization of the interaction energy. It is possible that in our driven system, the particles not only attempt to minimize their interaction energy, but at the same time organize into a pattern that maximizes the dissipation, since the ordered structures allow the particles to move at a speed close to the maximum velocity permitted by the driving. There have been proposals that driven self assembly processes can be understood as states that maximize the dissipation [69]. Futures directions could be to study the dissipation of the different configurations and determine whether the dissipation changes if the particles are forced to move in specified orbits rather than the orbits into which they naturally organize.

Other open questions include the nature of thermal melting transitions of the dynamical states, whether the states exhibit hysteresis across the boundaries of the phase diagrams in Figs. 8 and 14, and what the nature of the transitions among different pairs of phases

is. Some of the states we have described have similarities to magnetic or particle-based artificial spin ice configurations, so it could be interesting to explore the possible role of frustration, and whether it is the strongly frustrated cases that form mixed fluids. We considered two intermediate range and one long range particle-particle interaction potential, but it would be possible to explore other forms of interactions, such as dipolar interactions or particles with competing attractive and repulsive interactions. In this work we only addressed 50:50 mixtures of the two species, but it would be of interest to study different species ratios or the role of dopants, such as by switching the species identity of a small number of particles away from the 50:50 filling. It could also be interesting to introduce more than two particle species to see whether it is still possible for the system to form frozen states.

There are a number of possible ways to realize experimentally the dynamics we consider using particles that have an intermediate to long-range repulsion combined with some form of circular motion. These include spinning or circularly moving particles on the surface of a fluid, which are known to undergo pattern formation [70, 71]. Other examples include charged particles such as colloids with added chiral activity, charged particle systems on periodic trap arrays where the individual particle motion can be programmed, robotic systems, certain kinds of magnetic systems in which there are mixtures of different topological textures, and even coupled two-layer charge ordering systems with one type of circular drive on one layer and another drive on the other layer.

## XI. SUMMARY

We have proposed a new type of chiral system we call phase time crystals, which consists of two particle species with intermediate-to-long-range repulsion that undergo circular motion of the same chirality but out of phase by  $180^\circ$  between the species. We study a two-dimensional system of Bessel function, Yukawa, and Coulomb interacting particles that have activity in the form of circular driving. As a function of the driving frequency, which changes the size of the orbit, and the particle density, we find a remarkable variety of stable dynamical crystalline states. For high frequencies when the orbits are much smaller than the equilibrium particle spacing, there is a distorted triangular lattice. As the frequency decreases, the orbit size increases and the system forms a stripe-like crystal that becomes increasingly disordered as the orbits distort. A phase separation occurs when the frequency decreases further, allowing the particles to follow circular orbits that do not overlap. Once the frequency becomes low enough that the orbit of an individual particle is slightly larger than the average spacing between the static particles, a pairing of out of phase particles occurs in which each orbit contains one particle of each phase moving on opposite sides of the orbit, and the pairs

themselves order into a crystalline state. As the orbit size continues to increase with decreasing frequency, the paired crystal destabilizes into a phase-separated fluid state, and near certain ratios of the equilibrium lattice constant to the orbit size, we observe overlapping packed crystals and overlapping stripe crystals. At the lowest frequencies, the system forms a mixed fluid. We show that these states, including the paired crystal, are robust for a wide range of orbit sizes and densities as well as for all of the different particle interactions we consider.

For low-density systems where the effective particle-particle interactions are weaker, we find disordered states in which the individually orbiting particles have no long-range organization but the system is dynamically frozen in that there is no long-time diffusion. We show that the states we observe are robust against thermal fluctuations. In particular, the paired crystal persists up to the same temperature at which the non-driven crystal melts, and the pairs themselves are able to persist at higher temperatures in the form of a paired fluid. If we initialize the system in a random state, the transient times increase but the same phases still occur. If we change the driving so that the particles are counter-rotating instead of out of phase, the paired state does not occur and is replaced by chain lattice states where the particle species alternate along the chains. This provides a similar reduction in the pairwise interaction energy throughout the ac cycle as the out of phase particles achieved in the paired crystal state. If we use elliptical rather than circular driving for the out of phase particles, where the orientation of the ellipses is different for each species, we find a series of more complex states that we call molecular time crystals, which include states with spin ice ordering and states with superlattice ordering. The paired crystal states can still occur for elliptical driving, but the orbits only partially overlap to form a cross-like configuration.

We discuss how the states we observe can be considered as an extension of a time crystal, since they are periodic in both space and time. The system can be viewed as simultaneously minimizing the repulsive pairwise potential energy while also maximizing the dissipation or particle velocity. We also discuss how the organization of the system into dynamical frozen disordered states could be an example of an absorbing phase transition similar to the transitions to reversible states found in cyclically driven systems. Our results could be realized in systems with charge ordering, charged colloids, charged or magnetic particles at interfaces, bilayer systems, magnetic textures where there is also some form of circular driving, robotic systems, and mixtures of magnetic and charged particles.

## ACKNOWLEDGMENTS

We gratefully acknowledge the support of the U.S. Department of Energy through the LANL/LDRD program for this work. This work was supported by the US Department of Energy through the Los Alamos National

Laboratory. Los Alamos National Laboratory is operated by Triad National Security, LLC, for the National

Nuclear Security Administration of the U. S. Department of Energy (Contract No. 892333218NCA000001).

- 
- [1] C. A. Murray and D. H. Van Winkle, Experimental observation of two-stage melting in a classical two-dimensional screened Coulomb system, *Phys. Rev. Lett.* **58**, 1200 (1987).
- [2] A. Pertsinidis and X. S. Ling, Diffusion of point defects in two-dimensional colloidal crystals, *Nature (London)* **413**, 147 (2001).
- [3] A. Libál, C. Reichhardt, and C. J. O. Reichhardt, Point-defect dynamics in two-dimensional colloidal crystals, *Phys. Rev. E* **75**, 011403 (2007).
- [4] K. Zahn, R. Lenke, and G. Maret, Two-stage melting of paramagnetic colloidal crystals in two dimensions, *Phys. Rev. Lett.* **82**, 2721 (1999).
- [5] I. Guillamon, H. Suderow, A. Fernandez-Pacheco, J. Sese, R. Cordoba, J. M. De Teresa, M. R. Ibarra, and S. Vieira, Direct observation of melting in a two-dimensional superconducting vortex lattice, *Nature Phys.* **5**, 651 (2009).
- [6] X. Z. Yu, Y. Onose, N. Kanazawa, J. H. Park, J. H. Han, Y. Matsui, N. Nagaosa, and Y. Tokura, Real-space observation of a two-dimensional skyrmion crystal, *Nature (London)* **465**, 901 (2010).
- [7] Y. Tsui, M. He, Y. Hu, E. Lake, W. Taige, K. Watanabe, T. Taniguchi, M. Zaletel, and A. Yazdani, Direct observation of a magnetic-field-induced wigner crystal, *Nature (London)* **628**, 287 (2024).
- [8] H. Thomas, G. E. Morfill, V. Demmel, J. Goree, B. Feuerbacher, and D. Möhlmann, Plasma crystal: Coulomb crystallization in a dusty plasma, *Phys. Rev. Lett.* **73**, 652 (1994).
- [9] L. Lemelle, J.-F. Paliere, E. Chatre, and C. Place, Counterclockwise circular motion of bacteria swimming at the air-liquid interface, *J. Bacteriol.* **192**, 6307 (2010).
- [10] F. Kümmel, B. ten Hagen, R. Wittkowski, I. Buttinoni, R. Eichhorn, G. Volpe, H. Löwen, and C. Bechinger, Circular motion of asymmetric self-propelling particles, *Phys. Rev. Lett.* **110**, 198302 (2013).
- [11] N. H. P. Nguyen, D. Klotsa, M. Engel, and S. C. Glotzer, Emergent collective phenomena in a mixture of hard shapes through active rotation, *Phys. Rev. Lett.* **112**, 075701 (2014).
- [12] H. Löwen, Chirality in microswimmer motion: From circle swimmers to active turbulence, *Eur. Phys. J. Spec. Top.* **225**, 2319 (2016).
- [13] B. van Zuiden, J. Paulose, D. Irvine, W. Bartolo, and V. Vitelli, Spatiotemporal order and emergent edge currents in active spinner materials, *Proc. Natl. Acad. Sci. (USA)* **128**, 12919 (2016).
- [14] D. Banerjee, A. Souslov, A. G. Abanov, and V. Vitelli, Odd viscosity in chiral active fluids, *Nature Commun.* **8**, 1573 (2017).
- [15] M. Han, J. Yan, S. Granick, and E. Luijten, Effective temperature concept evaluated in an active colloid mixture, *Proc. Natl. Acad. Sci. (USA)* **114**, 7513 (2017).
- [16] V. Soni, E. S. Bililign, S. Magkiriadou, S. Sacanna, D. Bartolo, M. J. Shelley, and W. T. M. Irvine, The odd free surface flows of a colloidal chiral fluid, *Nature Phys.* **15**, 1188 (2019).
- [17] Q. L. Lei, M. P. Ciamarra, and R. Ni, Nonequilibrium strongly hyperuniform fluids of circle active particles with large local density fluctuations, *Sci. Adv.* **5**, eaau7423 (2019).
- [18] C. Reichhardt and C. J. O. Reichhardt, Reversibility, pattern formation, and edge transport in active chiral and passive disk mixtures, *J. Chem. Phys.* **150**, 064905 (2019).
- [19] B. Liebchen and D. Levis, Chiral active matter, *EPL* **139**, 67001 (2022).
- [20] T. H. Tan, A. Mietke, J. Li, Y. Chen, H. Higinbotham, P. J. Foster, S. Gokhale, J. Dunkel, and N. Fakhri, Odd dynamics of living chiral crystals, *Nature* **607**, 287 (2022).
- [21] P. Baconnier, D. Shohat, C. López, C. Coulais, V. Démery, G. Düring, and O. Dauchot, Selective and collective actuation in active solids, *Nature Phys.* **18**, 1234 (2022).
- [22] M. Fruchart, C. Scheibner, and V. Vitelli, Odd viscosity and odd elasticity, *Ann. Rev. Condens. Matter Phys.* **14**, 471 (2023).
- [23] M. Gelvan, A. Chirko, J. Kirpich, Y. Lavie, N. Israel, and N. Oppenheimer, Hydrodynamic spin-pairing and active polymerization of oppositely spinning rotors, *Nature Commun.* **16**, 10368 (2025).
- [24] L. Caprini, A. Petrini, and U. Marconi, Modeling chiral active particles: from circular motion to odd interactions, *J. Stat. Mech.* , 024001 (2026).
- [25] M. Han, M. Fruchart, C. Scheibner, S. Vaikuntanathan, J. J. de Pablo, and V. Vitelli, Fluctuating hydrodynamics of chiral active fluids, *Nature Phys.* **17**, 1260 (2021).
- [26] C. J. O. Reichhardt and C. Reichhardt, Active rheology in odd-viscosity systems, *EPL* **137**, 66004 (2022).
- [27] Z. Huang, M. te Vrugt, R. Wittkowski, and H. Löwen, Anomalous grain dynamics and grain locomotion of odd crystals, *Proc. Natl. Acad. Sci. (USA)* **122**, e2511350122 (2025).
- [28] H. Massana-Cid, D. Levis, R. J. H. Hernández, I. Pagonabarraga, and P. Tierno, Arrested phase separation in chiral fluids of colloidal spinners, *Phys. Rev. Res.* **3**, L042021 (2021).
- [29] E. S. Bililign, F. B. Usabiaga, Y. A. Ganan, A. Poncet, V. Soni, S. Magkiriadou, M. J. Shelley, D. Bartolo, and W. T. M. Irvine, Motile dislocations knead odd crystals into whorls, *Nature Phys.* **18**, 212 (2022).
- [30] R. Guo, J. Li, and B. Ai, Chirality-induced phase separation and collective dynamics in binary mixtures of chiral particles, *Phys. Rev. E* **111**, 045423 (2025).
- [31] B. Zhang and A. Snezhko, Hyperuniform active chiral fluids with tunable internal structure, *Phys. Rev. Lett.* **128**, 218002 (2022).
- [32] K. Jeong, Y. Kuroda, Y. Asatani, T. Kawasaki, and K. Miyazaki, Crystallization of chiral active Brownian particles at low densities, *Phys. Rev. Res.* **7**, 043212 (2025).
- [33] J. Wang, Z. Sun, H. Chen, G. Wang, D. Chen, G. Chen,

- J. Shuai, M. Yang, Y. Jiao, and L. Liu, Hyperuniform networks of active magnetic robotic spinners, *Phys. Rev. Lett.* **134**, 248301 (2025).
- [34] T. Kiechl, A. Altshuler, A. Lüders, Y. Roichman, and T. Franosch, Free chiral self-propelled robots compared to active Brownian circle swimmers, *Phys. Rev. E* **113**, 045409 (2026).
- [35] A. Aubret, M. Youssef, S. Sacanna, and J. Palacci, Targeted assembly and synchronization of self-spinning microgears, *Nature Phys.* **14**, 1114 (2018).
- [36] C. B. Caporusso, G. Gonnella, and D. Levis, Phase coexistence and edge currents in the chiral Lennard-Jones fluid, *Phys. Rev. Lett.* **132**, 168201 (2024).
- [37] J. Li, R. Guo, and B. Ai, Spontaneous separation of attractive chiral mixtures, *Phys. Rev. E* **110**, 024608 (2024).
- [38] H. Massana-Cid, C. Maggi, N. Gnan, G. Frangipane, and R. Di Leonardo, Multiple temperatures and melting of a colloidal active crystal, *Nat. Commun.* **15**, 6574 (2025).
- [39] N. Sungar, J. Sharpe, L. Ijzerman, and J.-W. Barotta, Synchronization and self-assembly of free capillary spinners, *Phys. Rev. E* **111**, 035104 (2025).
- [40] P. W. A. Vyas, A. D. and Schönhöfer, T. M. Hopkins, A. D. Hollingsworth, S. Sacanna, S. C. Glotzer, and P. Chaikin, Two-dimensional non-equilibrium melting of charged colloids, *Nature Phys.* **22**, 287 (2026).
- [41] C. C. de Souza Silva, M. V. Correia, and J. C. P. Velásquez, Emergent self-propulsion of skyrmionic matter in synthetic antiferromagnets, *Phys. Rev. Lett.* **135**, 086701 (2025).
- [42] C. Nisoli, R. Moessner, and P. Schiffer, Colloquium: Artificial spin ice: Designing and imaging magnetic frustration, *Rev. Mod. Phys.* **85**, 1473 (2013).
- [43] A. Ortiz-Ambriz, C. Nisoli, C. Reichhardt, C. J. O. Reichhardt, and P. Tierno, Colloquium: Ice rule and emergent frustration in particle ice and beyond, *Rev. Mod. Phys.* **91**, 041003 (2019).
- [44] F. Wilczek, Quantum time crystals, *Phys. Rev. Lett.* **109**, 160401 (2012).
- [45] A. Shapere and F. Wilczek, Classical time crystals, *Phys. Rev. Lett.* **109**, 160402 (2012).
- [46] P. Bruno, Impossibility of spontaneously rotating time crystals: A no-go theorem, *Phys. Rev. Lett.* **111**, 070402 (2013).
- [47] N. Y. Yao, C. Nayak, L. Balents, and M. P. Zaletel, Classical discrete time crystals, *Nature Phys.* **16**, 43 (2020).
- [48] Z. G. Nicolaou and A. E. Motter, Anharmonic classical time crystals: A resonance pattern formation mechanism, *Phys. Rev. Res.* **3**, 023106 (2021).
- [49] H. Zhao and I. Smalyukh, Space-time crystals from particle-like topological solitons, *Nature Mater.* **24**, 1802 (2025).
- [50] M. C. Morrell, L. Elliott, and D. G. Grier, Nonreciprocal wave-mediated interactions power a classical time crystal, *Phys. Rev. Lett.* **136**, 057201 (2026).
- [51] G. Liu, J. Bai, M. Baggioli, and J. Zhang, Three-stage melting of a macroscopic continuous spacetime crystal, *arXiv:2603.09649* (2026).
- [52] A. Libál, T. Balázs, C. Reichhardt, and C. J. O. Reichhardt, Colloidal dynamics on a choreographic time crystal, *Phys. Rev. Lett.* **124**, 208004 (2020).
- [53] A. Ernst, A. M. E. B. Rossi, and T. M. Fischer, Adiabatic and irreversible classical discrete time crystals, *SciPost Phys.* **13**, 091 (2022).
- [54] C. Reichhardt and C. J. O. Reichhardt, Depinning and nonequilibrium dynamic phases of particle assemblies driven over random and ordered substrates: a review, *Rep. Prog. Phys.* **80**, 026501 (2017).
- [55] J. Lekner, Summation of Coulomb fields in computer-simulated disordered-systems, *Physica A* **176**, 485 (1991).
- [56] N. Grønbech-Jensen, Lekner summation of long range interactions in periodic systems, *Int. J. Mod. Phys. C* **8**, 1287 (1997).
- [57] C. Reichhardt and C. J. O. Reichhardt, Nonlinear dynamics, avalanches, and noise for driven Wigner crystals, *Phys. Rev. B* **106**, 235417 (2022).
- [58] See supplemental material for animations showing the motion of the particles.
- [59] G. Malescio and G. Pellicane, Stripe phases from isotropic repulsive interactions, *Nature Mater.* **2**, 97 (2003).
- [60] M. A. Glaser, G. M. Grason, R. D. Kamien, A. Kosmrlj, C. D. Santangelo, and P. Zihlerl, Soft spheres make more mesophases, *EPL* **78**, 46004 (2007).
- [61] M. M. Fogler, A. A. Koulakov, and B. I. Shklovskii, Ground state of a two-dimensional electron liquid in a weak magnetic field, *Phys. Rev. B* **54**, 1853 (1996).
- [62] F. Sciortino, S. Mossa, E. Zaccarelli, and P. Tartaglia, Equilibrium cluster phases and low-density arrested disordered states: The role of short-range attraction and long-range repulsion, *Phys. Rev. Lett.* **93**, 055701 (2004).
- [63] C. J. Olson Reichhardt, C. Reichhardt, and A. R. Bishop, Structural transitions, melting, and intermediate phases for stripe- and clump-forming systems, *Phys. Rev. E* **82**, 041502 (2010).
- [64] A. Hooshanginejad, J.-W. Barotta, V. Spradlin, G. Pucci, R. Hunt, and D. M. Harris, Interactions and pattern formation in a macroscopic magnetocapillary salt system of mermaid cereal, *Nature Commun.* **15**, 5466 (2024).
- [65] C. Reichhardt, I. Regev, K. Dahmen, S. Okuma, and C. J. Olson Reichhardt, Reversible to irreversible transitions in periodic driven many-body systems and future directions for classical and quantum system, *Phys. Rev. Res.* **5**, 021001 (2023).
- [66] L. Corte, P. M. Chaikin, J. P. Gollub, and D. J. Pine, Random organization in periodically driven systems, *Nature Phys.* **4**, 420 (2008).
- [67] I. Regev, T. Lookman, and C. Reichhardt, Onset of irreversibility and chaos in amorphous solids under periodic shear, *Phys. Rev. E* **88**, 062401 (2013).
- [68] N. C. Keim, J. D. Paulsen, Z. Zeravcic, S. Sastry, and S. R. Nagel, Memory formation in matter, *Rev. Mod. Phys.* **91**, 035002 (2019).
- [69] J. England, Dissipative adaptation in driven self-assembly, *Nature Nanotech.* **10**, 919 (2015).
- [70] B. A. Grzybowski, X. Jiang, H. A. Stone, and G. M. Whitesides, Dynamic, self-assembled aggregates of magnetized, millimeter-sized objects rotating at the liquid-air interface: Macroscopic, two-dimensional classical artificial atoms and molecules, *Phys. Rev. E* **64**, 011603 (2001).
- [71] Y. Goto and H. Tanaka, Purely hydrodynamic ordering of rotating disks at a finite reynolds number, *Nature Commun.* **6**, 5994 (2015).